DETECTION LIMITS IN NANOMECHANICAL MASS FLOW SENSING FOR NANOFLUIDICS WITH NANOWIRE OPEN CHANNELS

Javier E. Escobar†, Juan Molina†, Eduardo Gil-Santos, José J. Ruz, Óscar Malvar, Priscila M. Kosaka, Javier Tamayo, Álvaro San Paulo, and Montserrat Calleja*
Instituto de Micro y Nanotecnología, IMN-CNM, CSIC (CEI UAM+CSIC), SPAIN
†These authors contributed equally.

ABSTRACT

Nanomechanical sensing is applied to measure the transport of liquid along the external surface of nanowire open fluidic channels. We integrate nanowire open channels with microcantilever resonators as sensors, enabling larger flow measurements; or use the nanowires simultaneously as open channels and resonators, for quantifying extremely small amounts of liquid. We study the detection limits of both systems and their implications for measuring the transport of ionic liquid from a microdroplet reservoir to Si nanowires when these are partially inserted into the microdroplet in the absence of any electrical signal. We obtain detection limits in the order of tens of femtogram and single attograms for each system, respectively, and a combined sensing range from 1 ag to beyond 10 pg, enabling the detection of transport of liquid volumes down to the zeptoliter scale.

KEYWORDS

Semiconductor nanowires, NEMS, nanomechanical resonators, nanofluidics, open fluidics, ionic liquids.

INTRODUCTION

Closed nanofluidic systems, such as channels, nozzles, or tubes, where fluids are enclosed by solid structures, are commonly used for the control of liquids [1]. Open systems, in which the liquid moves along the outer surface of a solid channel, are consolidating as an alternative bioinspired technological approach that provides otherwise impossible functionalities [2], especially for extremely miniaturized liquid handling [3]. Nanomechanical resonators [4], firmly established as ultra-high resolution mass sensors [5], can be integrated with open fluidics to obtain a quantitative measurement of flow rate in open systems with an unprecedented precision.

In this work we analyze the detection limits of two different realizations of this approach: first, a microcantilever-nanowire (MC-NW) device designed to allow larger flow measurements; and second, a nanowire-alone (NW-A) device that offers a much higher mass sensing resolution. Our study compares the fundamental mass detection limit of both devices with the actual resolution derived from their experimental frequency stability, and analyzes their sensing performance for

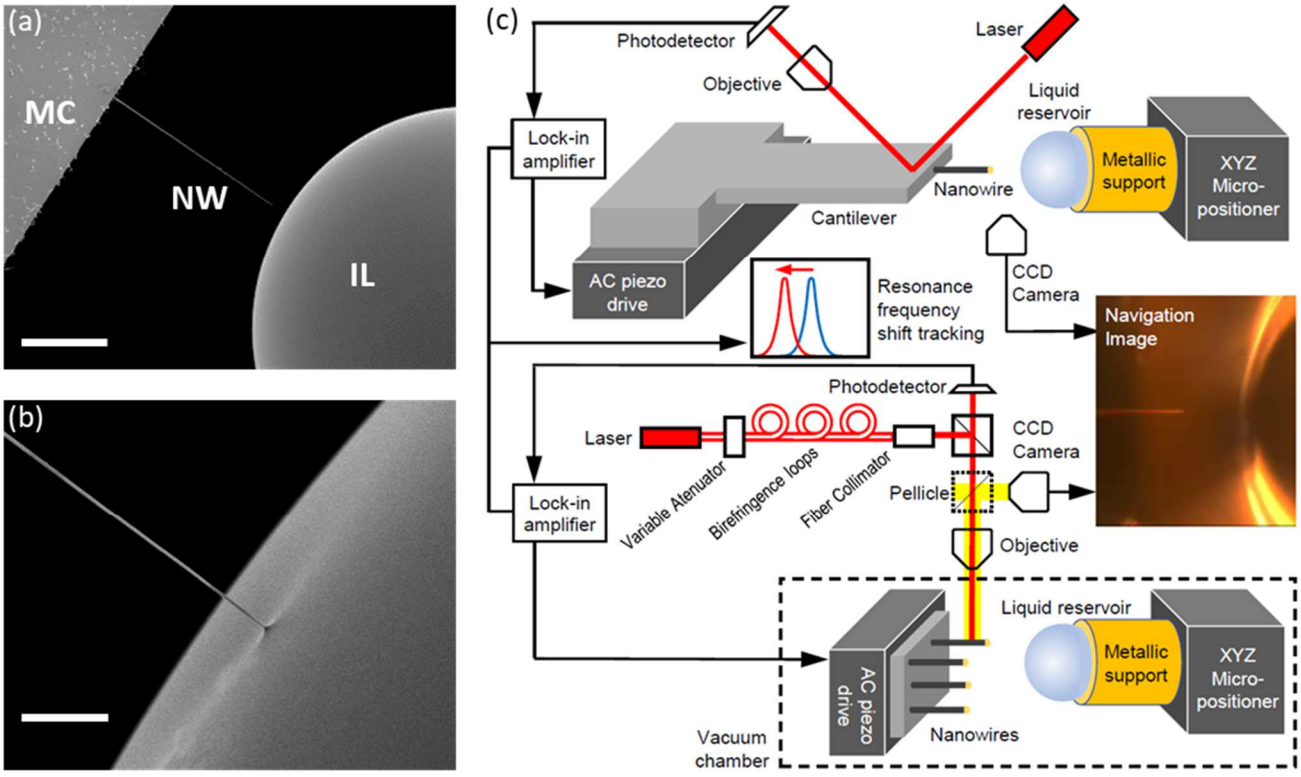

Figure 1: Nanomechanical mass flow sensing measurement setup. (a) SEM image of a MC-NW device placed in proximity of an ionic liquid microdroplet reservoir; scale bar: 20 μm. (b) SEM image showing a partial insertion of a nanowire into the ionic liquid microdroplet reservoir; scale bar: 2 μm. (c) Schematic depiction of experimental setup and resonance frequency tracking based on laser beam deflection transduction for the MC-NW device (upper section) and on laser beam scattering modulation for the NW-A device (lower section).

measuring the transport of ionic liquids (ILs) to the NWs when they are partially inserted into a microscopic IL reservoir in the absence of any electrical signal. We also determine the mass detection range of the devices by analyzing how the coupling between MC and NW in the MC-NW device limits its upper boundary.

RESULTS

Device design, fabrication and operation

The Si NWs used as open nanofluidic channels were grown by the VLS mechanism in an atmospheric pressure chemical vapor deposition reactor with $SiCl_4$ as precursor gas and 150-250 nm diameter colloidal Au nanoparticles (NPs) as growth catalyst [6]. Typical NW lengths are in the 30-50 μm range, base diameters of 150-470 nm and tip diameters of 30-270 nm. The MC-NW devices consist of a Si MC with its longitudinal axis oriented along a (111) crystallographic direction, where Si NWs are grown after random deposition of the Au catalyst NPs. These are conveniently diluted to obtain no more than one single NW at the edge of the MC (Figure 1a). The MCs have a length of 500 μm, a width of 90 μm and a thickness of 1-2 μm. The NW-A devices consist of VLS Si NWs vertically grown on a raw Si (111) substrate, with a previous step in which Au catalyst NPs are placed at desired positions near one edge of the substrate by nano-pipetting.

The IL reservoir is a microdroplet of DMPI-TFSI or DEME-TFSI placed on a metallic support that is mounted on a micro-positioning stage, which enables controlled insertions of the NW tip of around 1 μm (Figure 1b). This insertion length is small compared to our typical device length, allowing to relate a shift in its resonance frequency, Δf_R, to a liquid mass deposited near its tip, Δm_L, by the expression

$$\Delta m_L = -2 m_R \, \Delta f_R / f_R, \qquad (1)$$

where m_R and f_R are, respectively, the effective mass and resonance frequency of the resonator device before the insertion [7]. The effective mass of the NW-A device can be calculated as described in [6]. A similar approach to that followed in [8] can be applied to obtain m_R for the non-uniform cross section MC-NW device: interestingly, for the typical dimensions specified above, the only significant contribution of the NW to the total MC effective mass is given by the position of the added mass, placed away from the free end of the MC to the tip of the NW. This results in a 20% decrease in m_R.

In order to determine Δf_R, the resonance frequency of the fundamental flexural mode is measured before and after each insertion. Laser beam deflection readout is used for the MC-NW implementation, whereas scattering modulation [9] is used for the NW-A resonator (Figure 1c). Piezo-acoustic driving is used in both cases. Resonance frequency tracking is performed via phase-locked loop. MC-NW devices are operated in air, whereas NW-A devices are placed in a high vacuum chamber at 10^{-5} mbar; both at room temperature conditions. Typical values of fundamental resonance frequency f_R and quality factor Q are around 5-15 kHz and 10-50 for the MCs, and around 200-300 kHz and 7,000-40,000 for the NWs.

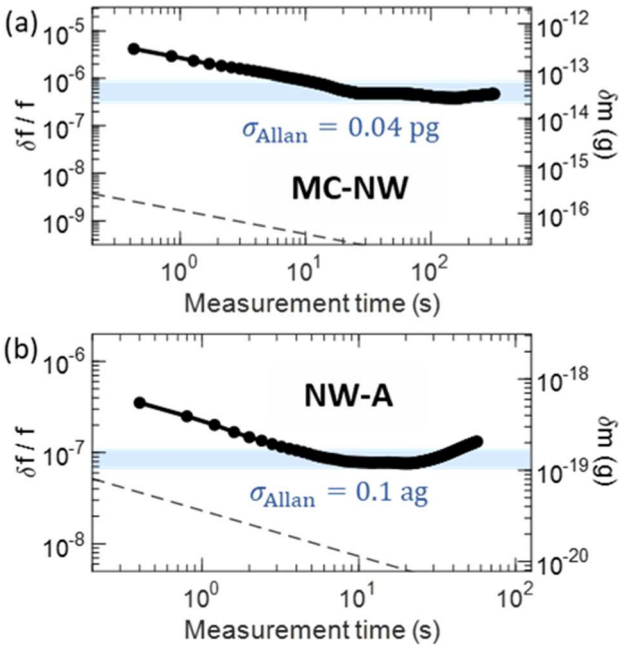

Figure 2: Experimental Allan deviation of resonance frequency as a function of measurement time (solid lines) for the MC-NW device (a) and for the NW-A device (b). The right axes use the effective mass of each device to convert frequency stability into minimum detectable mass. The dashed lines represent the fundamental limit.

Device performance and detection limits

Figure 2 shows measurements of Allan deviation performed to study the frequency stability $\delta f/f$ of our resonators [10]. At the measurement times of interest regarding our experiments (1-100 s), the Allan deviation takes values below 1 and 0.1 ppm for the MC-NW and NW-A devices, respectively; which can be converted into minimum detectable mass δm through equation 1. This results in experimental limits of 0.04 pg and 0.1 ag (see blue areas and right axes of Figure 2). Thus, the NW-A device provides a much higher mass resolution, mostly as a consequence of its much lower effective mass. The fundamental mass detection limit in δm was calculated as described in [6], and it is also plotted in the graphs for comparison (dashed lines). This theoretical value considers that the resonators are driven to their onset of nonlinearity and that thermomechanical noise is the dominant noise source. The calculation for the MC-NW considers that the added mass is located at the tip of the NW instead of the free end of the MC, which results into a 12% decrease in δm, mainly due to the 20% reduction in m_R discussed above. At short measurement times (< 10 s), the Allan deviation of the MC-NW device is three orders of magnitude higher than the fundamental limit. This difference is attributed to the fact that the full intrinsic mechanical dynamic range (DR) of the resonator is not accessed. At the lower DR boundary, the low Q resulting from operation in air makes instrumental noise dominate over thermomechanical noise. The upper DR boundary is also limited because the resonator is not driven up to its onset of nonlinearity, but around one order of magnitude lower due to piezo-drive power limitations. Vacuum operation to increase Q and instrumental improvements would reduce the difference between experimental and

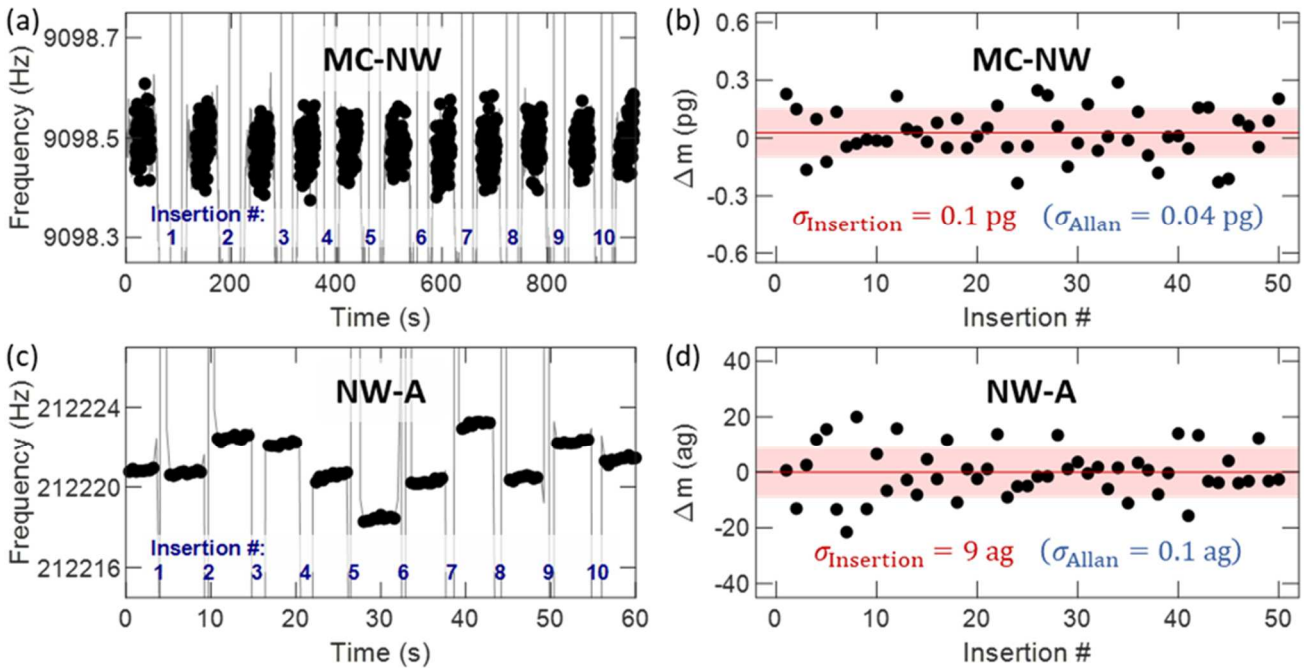

Figure 3: Effect of repeated insertions of NW tip into IL reservoir. (a) Example of resonance frequency tracking during a series of 10 iterated insertions of 20 s for the MC-NW device from Figure 2a, showing a negligible effect on the measured signal after each insertion event. The thin line represents all experimental values, including those for which the acquired signal is lost during insertion time, whereas dots only indicate the points from which the average frequency is calculated before and after each insertion. (b) Effective mass shift calculated from the tracked frequency of the MC-NW device after 50 iterated insertions. The red line indicates an average value of 0.03 pg and the red area represents a standard deviation of 0.1 pg. (c) Example of resonance frequency tracking during a series of 10 iterated insertions of 1 s for the NW-A device from Figure 2b, showing a clear effect of insertion events on the acquired signal after applying the same analysis as in (a). (d) Effective mass shift calculated from the tracked frequency of the NW-A device after 50 iterated insertions. The red line indicates an average value of -0.1 ag and the red area represents a standard deviation of 9 ag.

theoretical limits. Regarding the NW-A device, thermomechanical noise can be properly resolved in vacuum, pushing its Allan deviation only one order of magnitude above the fundamental limit. Increasing piezo drive up to the onset of nonlinearity would improve the experimental limit of both devices at short measurement times, but it could also compromise frequency stability at longer times.

We now analyze the implications of these detection limits for measuring the transport of IL from a microdroplet reservoir to the tip of NWs when these are repeatedly inserted into the IL reservoir in the absence of any applied electrical signal. Previous work has determined that in such conditions, a precursor film of a few nm thickness is expected to spread spontaneously on the NW surface, but no additional flow happens without applying a bias voltage between the IL reservoir and the NW [3]. Figure 3a shows that for the MC-NW device, the resonance frequency before each insertion does not significantly change when it is measured after the insertion (the signal is not tracked during insertion). If we convert these small frequency shifts into deposited mass Δm_L through equation 1, we obtain the series shown in Figure 3b (extended to 50 insertion events). The standard deviation $\sigma_{Insertion}$ with respect to the 0.03 pg average deposited mass obtained from this series is 0.1 pg, which is comparable to the detection limit established by σ_{Allan}. Since the average value lies below both σ_{Allan} and $\sigma_{Insertion}$, we conclude that any IL mass transferred during the insertions is not sufficiently above the detection limit of the MC-NW device to provide meaningful measurements. We perform the same analysis on the NW-A system (Figure 3c-d), finding a remarkable difference. For this device, the signal is clearly shifted after each insertion, which translates into an average transported mass of -0.1 ag and a $\sigma_{Insertion}$ of 9 ag, almost two orders of magnitude above σ_{Allan}. On the one hand, the negligible average value is consistent with the expectation of no liquid flow at zero bias voltage [3]. But on the other hand, the increased dispersion well above σ_{Allan} is attributed to a real mass effect due to the adsorption and desorption of small amounts of liquid after each insertion. The mass resolution of the NW-A device allows to observe this effect, which is screened by frequency noise in the MC-NW device. We thus conclude that the NW-A device provides enough resolution to detect IL transfer in these conditions.

Figure 4a shows a characterization of $\sigma_{Insertion}$ as a function of tip diameter in 41 different NW-A devices, revealing a clear and steep positive correlation between both magnitudes. The observed correlation provides support for our interpretation of $\sigma_{Insertion}$ as a mass effect, as it is expected that wider NWs move larger IL masses. The thinnest NW tip diameter that we have tested is around 30 nm, providing a dispersion of around 1 ag. This value defines a lower experimental limit in the ability of our technology to measure liquid transport, which, converted into volume, lies in the single zeptoliter scale.

Finally, we estimate the upper limit of our sensing approach as the maximum added mass that the MC-NW

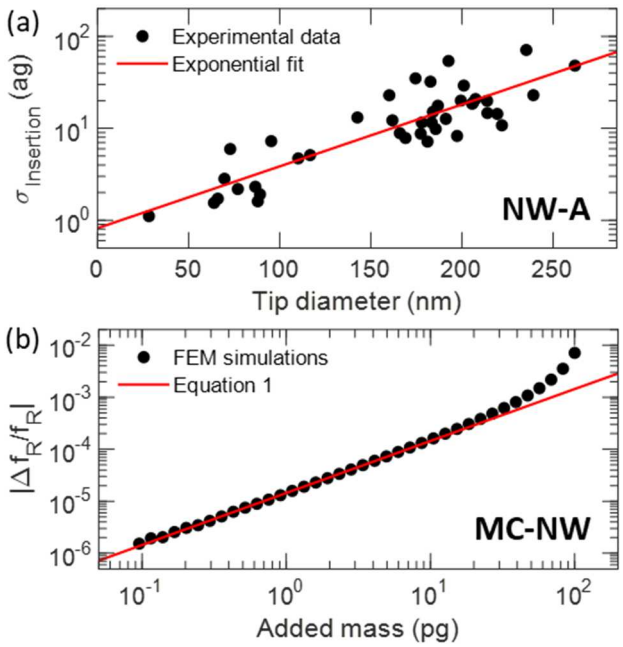

Figure 4: Liquid transport detection limits. (a) Insertion dispersion of 41 different NW-A devices as a function of tip diameter (black dots), showing a clear correlation between both magnitudes (an exponential fit is included in red as a guide to the eye). (b) Simulated frequency shift as a function of the amount of added mass at the tip of the NW in the MC-NW device (black dots), and comparison with the theoretical expression used in this work to convert frequency shift into effective mass (red line).

device can support within the framework of our analysis. Equation 1 does not have into account the coupling effect arising when, as a consequence of the added mass, the frequency of the fundamental flexural mode of the NW approximates that of the MC [11]. This phenomenon can be calculated by finite element simulations by varying the magnitude of a point mass located at the tip of the NW. Black dots in Figure 4b show the results of this simulation compared to the theoretical dependence expected if only equation 1 is considered (red line). The region where both curves diverge significantly, above a few tenths of pg, defines an upper limit for mass flow control where our method would not correctly determine the amount of liquid mass added. This upper limit could be further increased by designing MC and NW such that their fundamental flexural modes have more distant resonance frequencies.

CONCLUSION

The integration of nanomechanical resonators with open fluidics provides unprecedented tools for applications such as printing, patterning, constrained chemical reactions or bioassays. Our study of the mass detection limits of two particular implementations of these devices demonstrates their suitability for high resolution and high dynamic range mass flow sensing. After exploring the implications of such detection limits for measuring the transport of IL from a microdroplet reservoir to the tip of NWs as these are repeatedly inserted into the IL reservoir in the absence of any applied electrical signal, we find that the random adsorption and desorption of small amounts of liquid after each insertion can be resolved when the NWs are used both as channels and as sensors.

ACKNOWLEDGEMENTS

This work was supported by the ERC-CoG 681275 "LIQUIDMASS" and by the Spanish Science and Innovation Ministry through Projects "EXOFLUX" (PGC2018-101762-B-I00) and "MOMPs" (TEC2017-89765- R). We acknowledge the service from the MiNa Laboratory at IMN, and funding from CM (project S2018/NMT-4291 TEC2SPACE), MINECO (project CSIC13-4E-1794) and EU (FEDER, FSE). E.G.S. acknowledges financial support by the Spanish Science and Innovation Ministry through Ramón y Cajal grant RYC-2019-026626-I.

REFERENCES

[1] W. Sparreboom, A. van den Berg, and J. C. T. Eijkel, "Principles and applications of nanofluidic transport," *Nat. Nanotechnol.*, vol. 4, no. 11, pp. 713–720, 2009, doi: 10.1038/nnano.2009.332.

[2] C. T. Ertsgaard, D. Yoo, P. R. Christenson, D. J. Klemme, and S.-H. Oh, "Open-channel microfluidics via resonant wireless power transfer," *Nat. Commun. 2022 131*, vol. 13, no. 1, pp. 1–9, Apr. 2022, doi: 10.1038/s41467-022-29405-2.

[3] J. Y. Huang *et al.*, "Nanowire liquid pumps," *Nat. Nanotechnol. 2013 84*, vol. 8, no. 4, pp. 277–281, Mar. 2013, doi: 10.1038/nnano.2013.41.

[4] S. Schmid, L. G. Villanueva, and M. L. Roukes, *Fundamentals of nanomechanical resonators*, vol. 49. Springer, 2016.

[5] J. Chaste, A. Eichler, J. Moser, G. Ceballos, R. Rurali, and A. Bachtold, "A nanomechanical mass sensor with yoctogram resolution," *Nat. Nanotechnol.*, vol. 7, no. 5, pp. 301–304, 2012, doi: 10.1038/nnano.2012.42.

[6] J. Molina *et al.*, "High Dynamic Range Nanowire Resonators," *Nano Lett.*, vol. 21, no. 15, pp. 6617–6624, Aug. 2021, doi: 10.1021/acs.nanolett.1c02056.

[7] K. L. Ekinci, Y. T. Yang, and M. L. Roukes, "Ultimate limits to inertial mass sensing based upon nanoelectromechanical systems," *J. Appl. Phys.*, vol. 95, no. 5, pp. 2682–2689, Feb. 2004, doi: 10.1063/1.1642738.

[8] O. Malvar *et al.*, "Tapered silicon nanowires for enhanced nanomechanical sensing," *Appl. Phys. Lett.*, vol. 103, no. 3, Jul. 2013, doi: 10.1063/1.4813819.

[9] J. Molina *et al.*, "Optical Transduction for Vertical Nanowire Resonators," *Nano Lett.*, p. acs.nanolett.9b04909, Mar. 2020, doi: 10.1021/acs.nanolett.9b04909.

[10] M. Sansa *et al.*, "Frequency fluctuations in silicon nanoresonators," *Nat. Nanotechnol.*, vol. 11, no. 6, pp. 552–558, Jun. 2016, doi: 10.1038/nnano.2016.19.

[11] E. Gil-Santos *et al.*, "Optomechanical detection of vibration modes of a single bacterium," *Nat. Nanotechnol.*, vol. 15, no. 6, pp. 469–474, 2020, doi: 10.1038/s41565-020-0672-y.

CONTACT

*A. San Paulo, tel: +34 918060700;
alvaro.sanpaulo@csic.es